nature energy

SUPPLEMENTARY INFORMATION

https://doi.org/10.1038/s41560-017-0033-8

In the format provided by the authors and unedited.

Fire-extinguishing organic electrolytes for safe batteries

Jianhui Wang[1], Yuki Yamada[1,2], Keitaro Sodeyama[2,3,4], Eriko Watanabe[1], Koji Takada[1], Yoshitaka Tateyama[2,3] and Atsuo Yamada[1,2]*

[1]Department of Chemical System Engineering, The University of Tokyo, Bunkyo-ku, Tokyo 113-8656, Japan. [2]Elements Strategy Initiative for Catalysts & Batteries (ESICB), Kyoto University, Nishikyo-ku, Kyoto 615-8245, Japan. [3]Center for Green Research on Energy and Environmental Materials (GREEN) and Research and Services Division of Materials Data and Integrated System (MaDIS), National Institute for Materials Science (NIMS), Tsukuba, Ibaraki 305-0044, Japan. [4]PRESTO, Japan Science and Technology Agency (JST), Kawaguchi, Saitama 333-0012, Japan. *e-mail: yamada@chemsys.t.u-tokyo.ac.jp

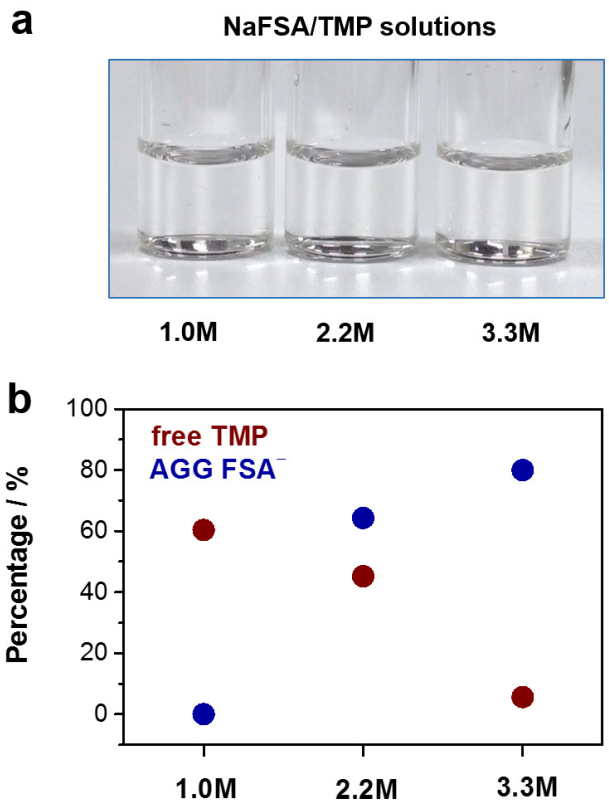

Supplementary Figure 1 | Lab-made NaFSA/TMP solutions and their structural information. a, A photo image of various concentrations of NaFSA/TMP solutions. **b**, Calculated percentage of free-state TMP solvents and aggregate-state FSA^- anions in different concentrations of NaFSA/TMP solutions obtained from DFT-MD simulations. Detail coordination information is shown in Supplementary Fig. 2.

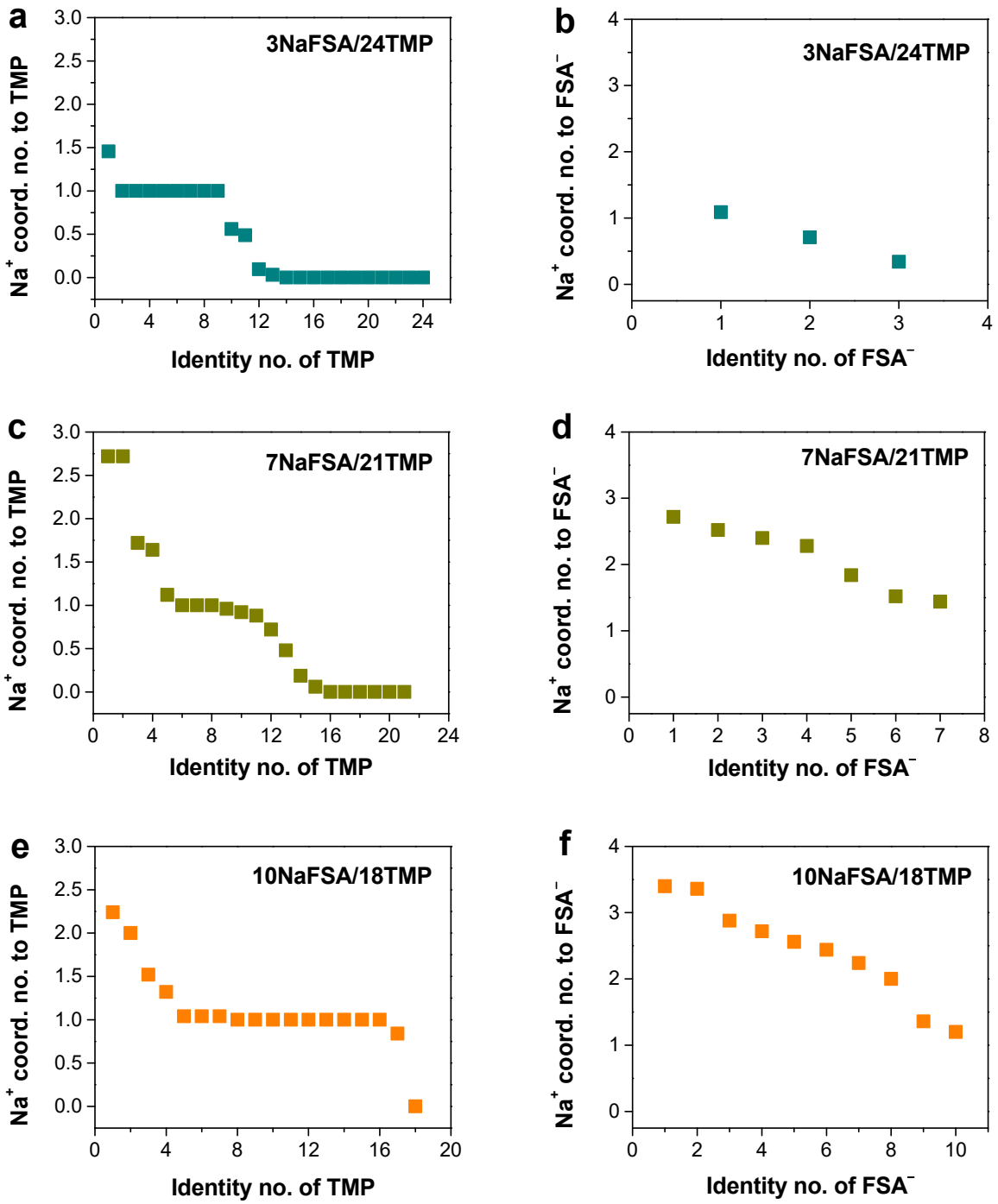

Supplementary Figure 2 | Coordination environment of Na^+ to solvents and anions in different concentrations of NaFSA/TMP solutions. a,**c**,**e**, Na^+ coordination numbers to TMP molecules; **b**,**d**,**f**, Na^+ coordination numbers to FSA^- anions. The coordination numbers are average values during all DFT-MD simulation time of 10 ps (100,000 steps × 0.1 fs interval). All TMP molecules and FSA^- anions are labeled with identity numbers.

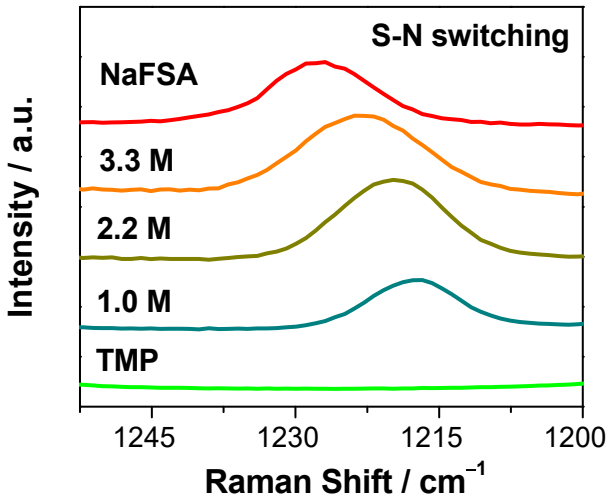

Supplementary Figure 3 | Raman spectra of the NaFSA/TMP solutions. Raman spectroscopy measurements were carried out on a NRS-5100 spectrometer with an exciting laser of 514 nm. The samples were examined in a quartz cell, which was sealed in the glove box without any contamination of air. Pure TMP solvent and NaFSA powder were used as references. Clearly, as the concentration increases, the FSA^- band shows a remarkable upshift. This typical feature evidences the intensified cation-anion association in the concentrated electrolyte via the formation of contact ion pairs and aggregate clusters as generally observed in the lithium ion concentrated electrolytes.[1–4]

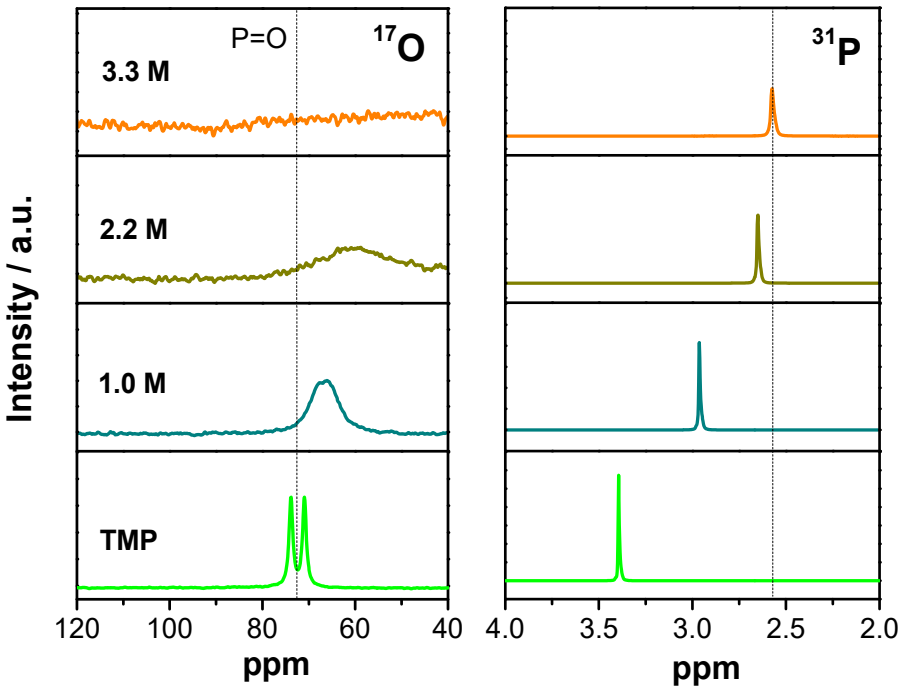

Supplementary Figure 4 | ^{17}O and ^{31}P NMR spectra of the NaFSA/TMP solutions. The samples were sealed in a glass tube and tested on a JNM-ECX400 spectrometer at room temperature. The ^{17}O NMR spectra were collected at a frequency of 54.2 MHz, using ^{17}O NMR of pure water as reference (0 ppm). The ^{31}P NMR spectra were collected at a frequency of 161.8 MHz, using ^{31}P of 85% H_3PO_4 as reference (0 ppm). For TMP molecules coordinated to Na^+ cation, both ^{17}O and ^{31}P peaks move towards upfield (1.0 M vs pure TMP), showing a shielding effect. As the salt concentration increases, these chemical shifts further move towards upfield, evidencing the strengthening interaction between TMP molecules and Na^+ cations. Similar phenomena was also observed in the electrolyte of LiFSA/DME.[5]

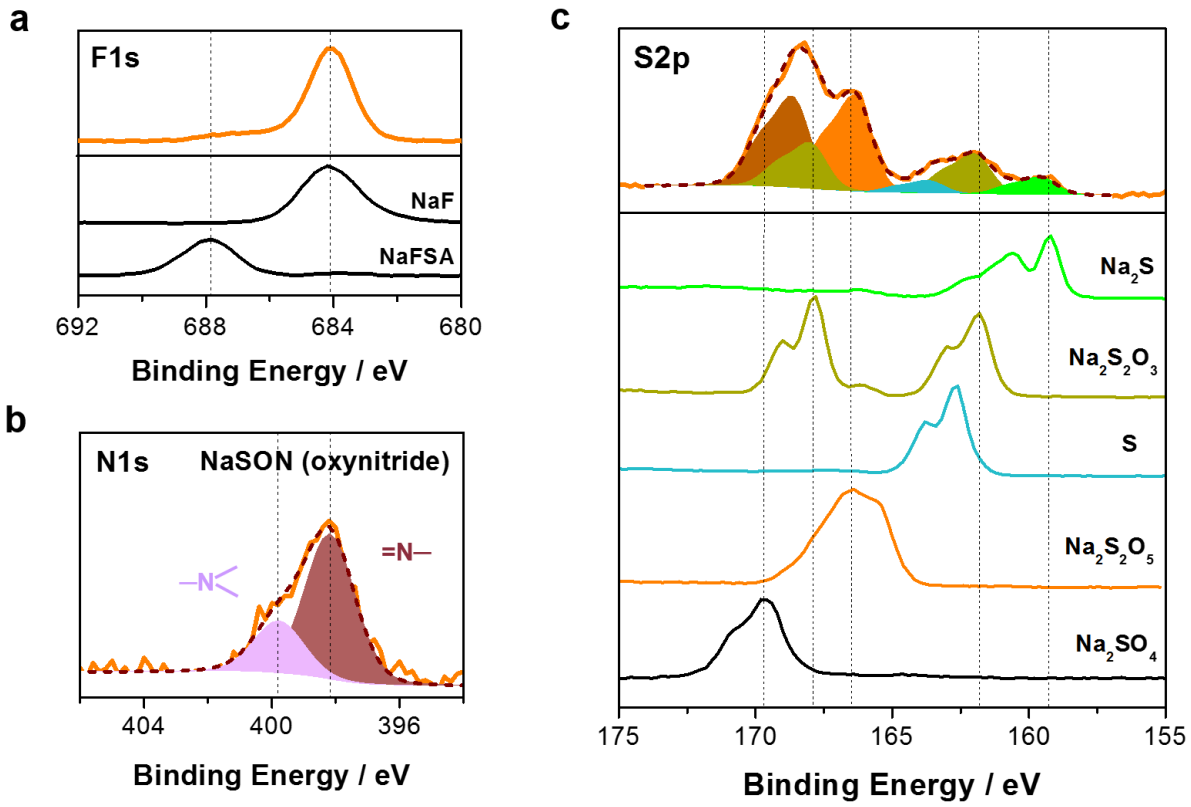

Supplementary Figure 5 | Identification of the passivation film generated in the concentrated electrolyte by XPS spectra. a-c are F1s, N1s and S2p spectra of the hard carbon electrode cycled in 3.3M NaFSA/TMP electrolyte, respectively. The F1s spectrum indicated the presence of NaF in the passivation film and the absence of residual NaFSA salt on the electrode surface. The N1s spectrum at ~398.3 eV revealed that nitrogen is in a negatively charged state in the passivation film, which rules out the possibility of some nitrite, nitrate or azide. Na_3N is also impossible because it is unstable at room temperature. Because the N-containing component comes from the reduction of NaFSA, we ascribed it as a sodium sulfur oxynitride (NaSON) based on three reasons: (1) the structure of NaSON resembling with that of NaFSA; (2) the detected binding energy of S2p (~398.3 eV) close to that of NaFSA (400.0 eV); (3) the detected N1s peak with an asymmetric feature in accord with that of lithium phosphorous oxynitride (LiPON) whose nitrogen has two kinds of local chemical environments.[6] While only one paper of sulfur oxynitride has been reported thus far with little structural information,[7] a further confirmation of this assumption is needed in future. The binding energy of S2p distributes in the range of 159~170 eV (referring to various chemical valences), indicating a complicated reduction of NaFSA. Considering the main elements of Na, S, O, N and F, the S-containing components possibly include NaSON, Na_2S, S, Na_2SO_3, Na_2SO_4, Na_2SO_5, $Na_2S_2O_3$, $Na_2S_2O_4$, $Na_2S_2O_5$, $Na_2S_2O_6$, $Na_2S_2O_7$, $Na_2S_2O_8$, polysulfide (Na_2S_{n+1}, n>1) and polythionate ($Na_2S_{n+2}O_6$, n>1). Na_2SO_5 and $Na_2S_2O_8$ are strong oxidizing agents, which cannot be compatible with the highly reducing environment. Na_2SO_3, $Na_2S_2O_4$ and $Na_2S_2O_7$ are ruled out based on the FTIR results (see Supplementary Fig. 6). Combing the results of XPS and ATR-FTIR spectra, the S-

containing compounds can be ascribed to be a composite of NaSON, $Na_2S_2O_5$, $Na_2S_2O_3$, Na_2S and S. The peak at ~168.7 eV could be contributed by the NaSON component. The content of Na_2SO_4 is small if any. Right now, the possibility of $Na_2S_2O_6$ cannot be ruled out because we have no FTIR and XPS data of it. Polysulfide (Na_2S_{n+1}, n>1) and polythionate ($Na_2S_{n+2}O_6$, n>1) are also possible, which could be regarded as the combination of sulfur (S) with sodium sulfide (Na_2S) or sodium dithionate ($Na_2S_2O_6$). XPS spectra of various references were shown, including of NaF (>99.0%), Na_2S (>97%), $Na_2S_2O_3$ (>99.0%), S (>99.99%), $Na_2S_2O_5$ (>99.0 %) and Na_2SO_4 (>99.0 %), which were all purchased from Sigma-Aldrich.

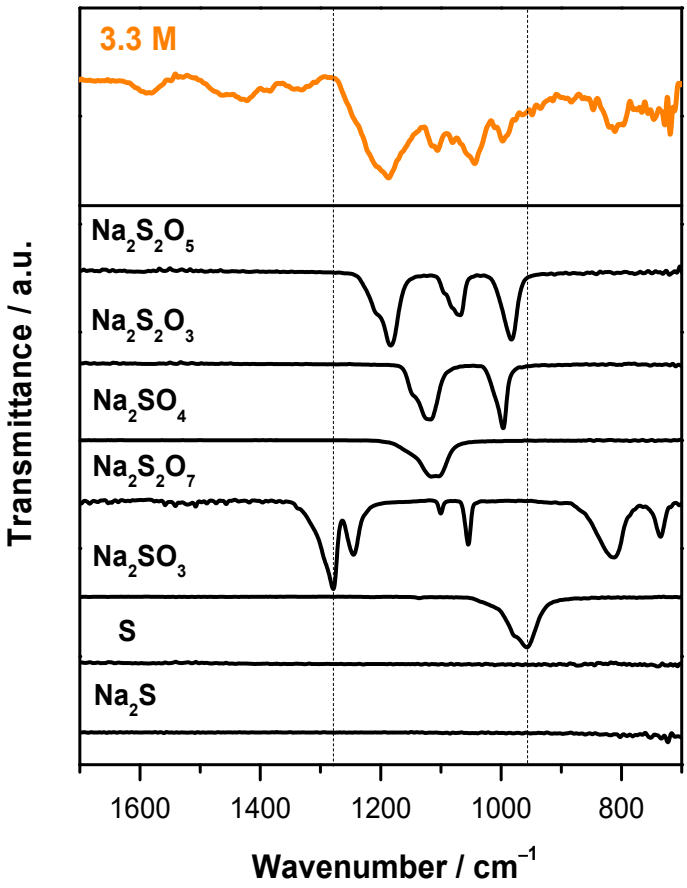

Supplementary Figure 6 | Identification of the passivation film generated in the concentrated electrolyte by ATR-FTIR spectra. ATR-FTIR spectrum was obtained on the reductively polarized Cu foil (to 0.01 V) in the 3.3 M NaFSA/TMP electrolyte. Here the polarized Cu foil was used because (1) our ATR-FTIR spectroscopy cannot get any IR signal directly from the black hard carbon electrode and (2) it has an essentially identical passivation film with that of the cycled hard carbon electrode (see Supplementary Fig. 7). Various pure sulfur-compounds are used as references. The ATR-FTIR result suggests the presence of $Na_2S_2O_5$ and $Na_2S_2O_3$ and the absence of $Na_2S_2O_7$ and Na_2SO_3 in the passivation film. Moreover, $Na_2S_2O_4$, which has a very strong infrared absorption peak at 912 cm^{-1} (obtained from an IR database[8]), can be ruled out as a component of the passivation film. Na_2SO_3 (>99.0%) was purchased from Sigma-Aldrich. $Na_2S_2O_7$ was synthesized by vacuuming $NaHSO_4.H_2O$ (>99.0%, Sigma-Aldrich) at 200 °C for 10 hours.

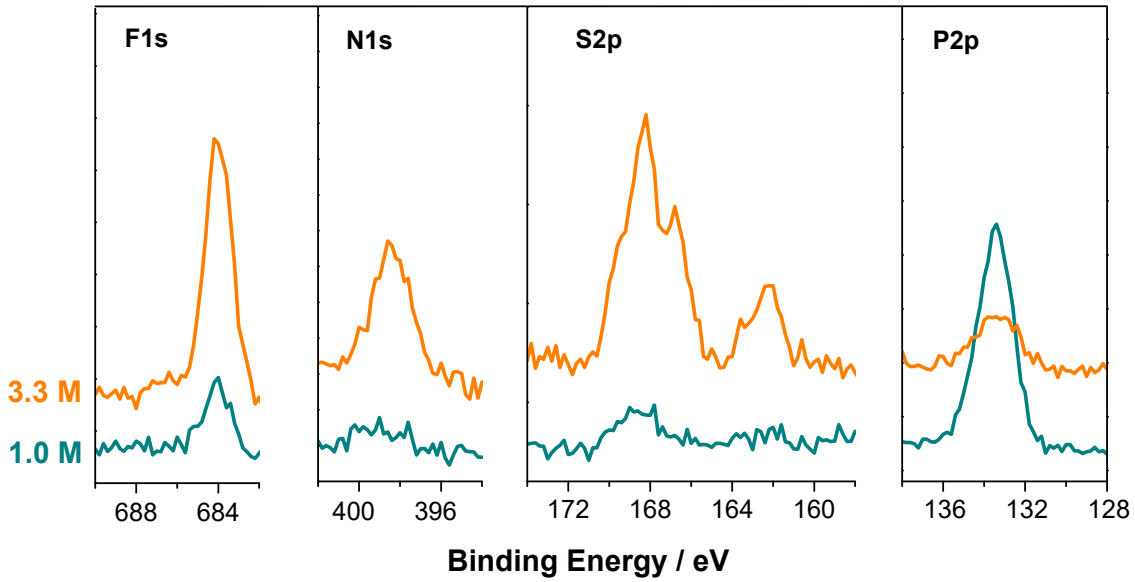

Supplementary Figure 7 | XPS spectra of Cu foils after a reductive polarization in the NaFSA/TMP electrolytes. These XPS spectra show very similar with those of cycled hard carbon electrodes, indicating that the polarized Cu foil has an essentially identical passivation film with that of the cycled hard carbon electrode.

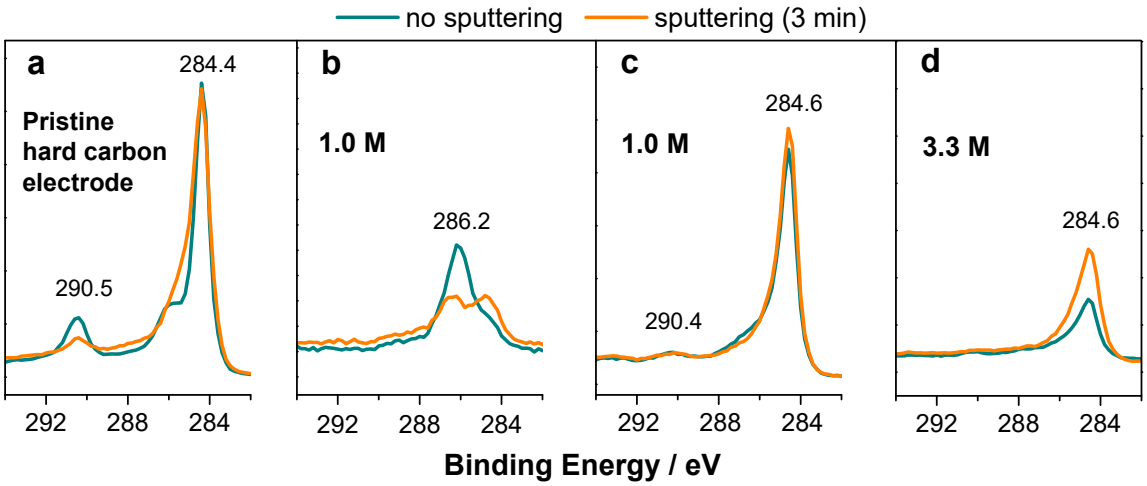

Supplementary Figure 8 | C1s XPS spectra of pristine and cycled hard carbon electrodes with/without Ar^+ sputtering. a, pristine hard carbon electrode. **b**,**c**, cycled electrodes in the 1.0 M NaFSA/TMP electrolyte. **d**, cycled hard carbon electrode in the 3.3 M NaFSA/TMP electrolyte. According to the SEM image (Fig. 4b in main text), the reduction products of 1.0 M NaFSA/TMP electrolyte showed elongate-block crystal particles with an inhomogenous distribution on the electrode surface. (**b**,**c**) show two representative results; the former should be from the reduction products of the electrolyte, while the latter should be from the exposed hard carbon electrode without a passivation. The C1s signal in (**d**) looks similar with those in (**a**,**c**) but different from that in (**b**), which thus should be mainly arisen from the hard carbon. Therefore, there is no significant content of carbon-containing compounds in the passivation film produced in the 3.3 M NaFSA/TMP electrolyte.

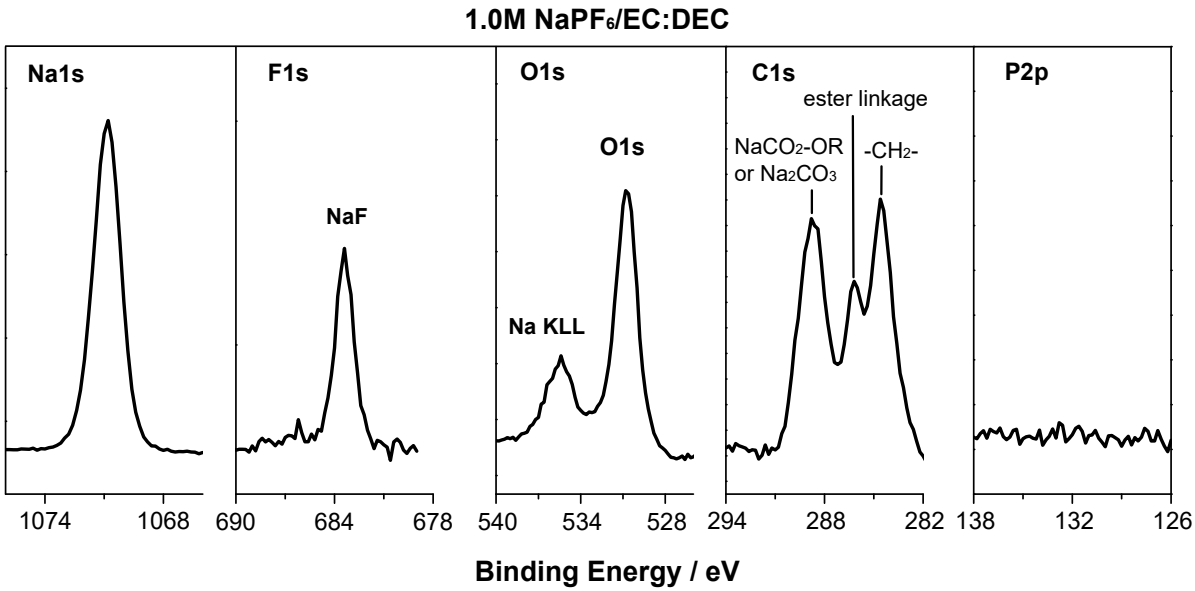

Supplementary Figure 9 | XPS spectra of the reductively polarized Cu foil in 1.0 M $NaPF_6$/EC:DEC. The C1s spectrum shows similar with a previous report.[9]

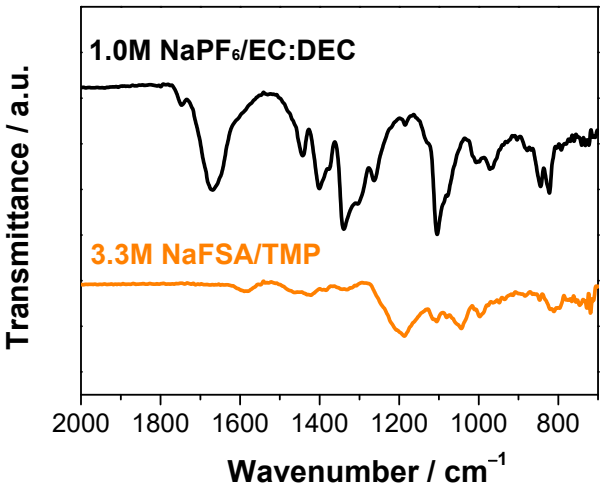

Supplementary Figure 10 | ATR-FTIR of the reductively polarized Cu foil in 1.0 M $NaPF_6$/EC:DEC. It shows a main product of sodium ethylene dicarbonate (NEDC), consistent with a previous report.[10] The content of Na_2CO_3 in the present work is small in the initial cycling; it would increase during cycling or at elevated temperatures due to the decomposition of the metastable NEDC. As a comparison, the ATR-FTIR spectrum of the passivation film produced in the concentrated electrolyte is also shown.

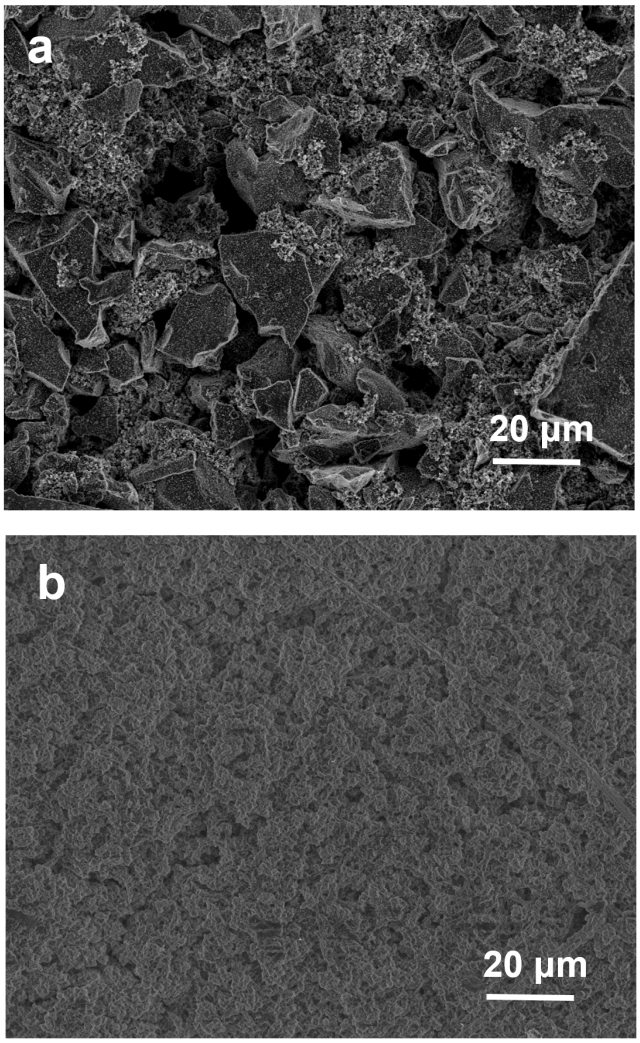

Supplementary Figure 11 | Surface morphology of hard carbon electrodes after a long-term cycling. a,b, SEM images of hard carbon electrodes after 850 cycles in the concentrated 3.3 M NaFSA/TMP electrolyte and 180 cycles in conventional 1.0 M $NaPF_6$/EC:DEC electrolyte, respectively. For the electrode cycled in the conventional electrolyte, hard carbon particles cannot be seen, showing a very thick surface film on it.

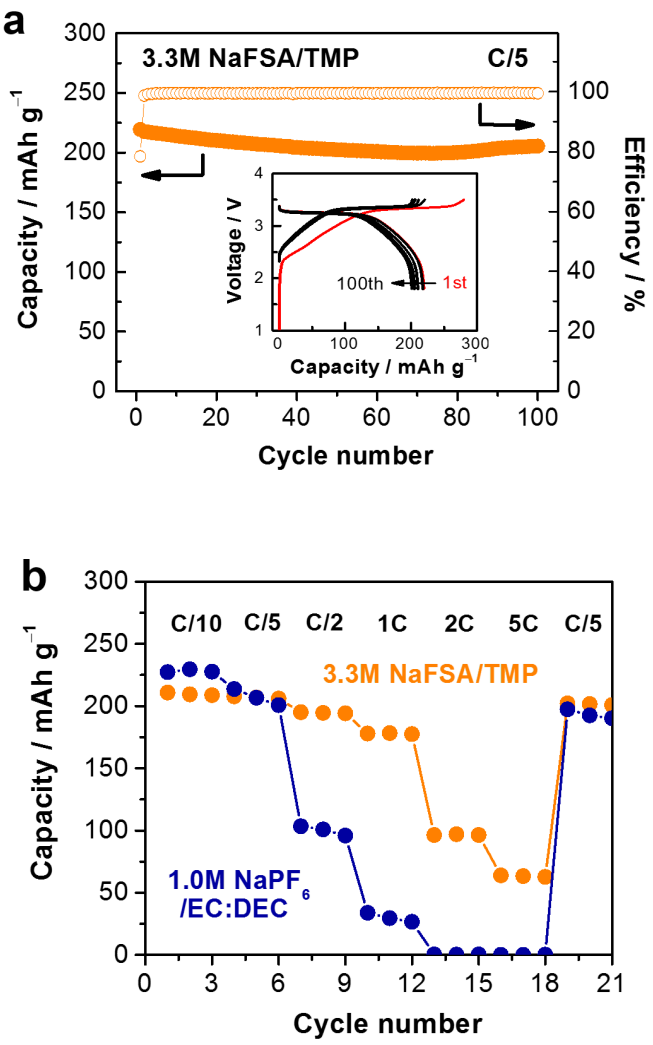

Supplementary Figure 12 | Electrochemical performance of a 3.2 V $Na_3V_2(PO_4)_3$ | hard carbon full cell. a, Cycling performance and coulombic efficiency of the full cell using 3.3 M NaFSA/TMP electrolyte at a C/5 rate. The inset shows the charge–discharge voltage curves. **b**, Discharge capacity of the full cell at various C-rates. Charge and discharge were conducted at the same C-rate at 25 °C with a cutoff voltage of 1.8–3.5 V. A 1C-rate corresponds to 250 mA g^{-1} on the weight basis of the hard carbon active material. The capacity is based on the hard carbon anode. Considering the capacity retention of 93% after 100 cycles, the coulombic efficiency should be over 99.92% theoretically. The obtained coulombic efficiency (99.5%) of the full cell is slightly lower than the theoretic value, which should be caused by a technical issue associated with coin-type cells, because our coin cell using both commercial electrode materials ($LiCoO_2$ and graphite) and electrolyte (1.0M $LiPF_6$/EC:DMC) still shows a similarly lower coulombic efficiency than the theoretic value. In the coin cell, the areal contact between the electrolyte with cell components (cathode/anode cases, spacer, spring, etc.) is much larger than that in commercial laminated cell. In addition, the separator, binder and conductive carbon are not optimized in our lab, which may also cause some trace parasitical reactions in the battery. Nevertheless, the

capacity retention is high and the charge-discharge curves show no significant change during 100 cycles under strict conditions of a limited Na^+ resource and a low rate (C/5), which indicate that those trace parasitical reactions in the full cell do not consume the active Na^+ resource. We think that the coulombic efficiency can be further improved by optimizing the cell design.

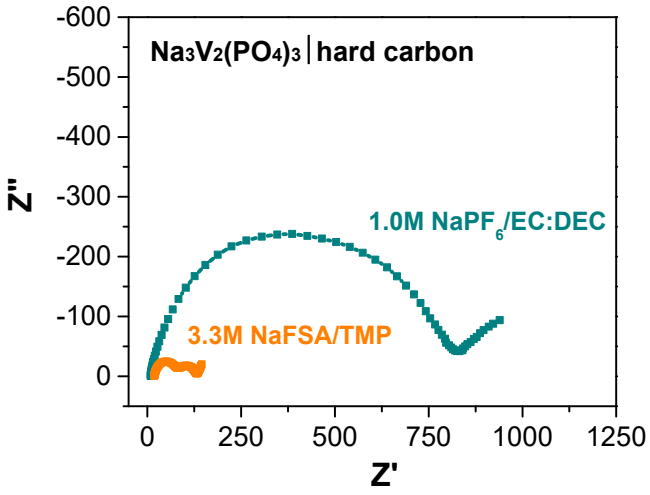

Supplementary Figure 13 | Electrochemical Impedance spectra of $Na_3V_2(PO_4)_3$ | hard carbon full cells using concentrated and conventional electrolytes. Impedance spectra were measured at 25 °C as a function of frequency using an AC impedance spectrometer (Solartron 147055BEC).

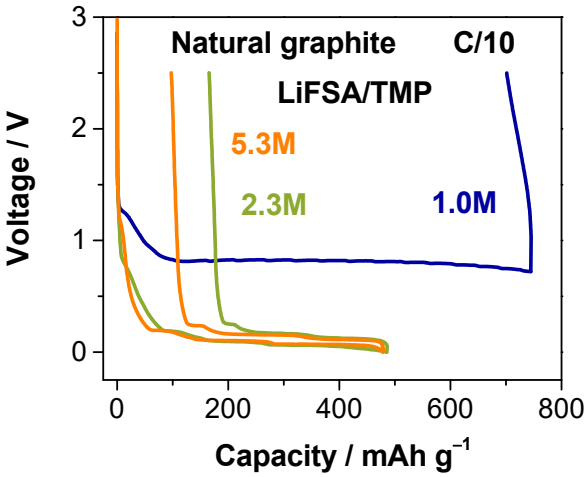

Supplementary Figure 14 | Initial charge-discharge profiles of natural graphite │lithium metal half-cells using various concentrations of LiFSA/TMP electrolytes. The dilute (1.0 M) electrolyte could not work with the graphite electrode at all while the concentrated (5.3 M) electrolyte realized reversible lithium de-/intercalation of the graphite electrode, which is similar with those observed in sodium-ion system that tested hard carbon electrodes in NaFSA/TMP electrolytes. The initial columbic efficiency for the 5.3 M LiFSA/TMP electrolyte on the natural graphite electrode was 79.6%. Most recently, we found that this initial columbic efficiency could be remarkably improved to over 95% with a commercially used artificial graphite electrode (see Supplementary Fig. 15). A 1C-rate corresponds to 372 mA g^{-1} on the weight basis of the graphite active material.

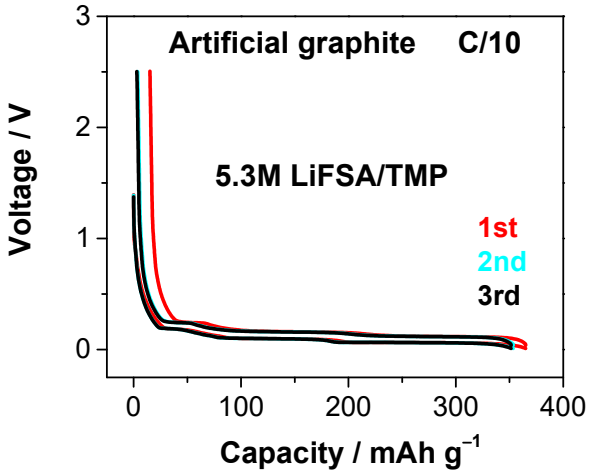

Supplementary Figure 15 | First three charge-discharge profiles of artificial graphite │lithium metal half-cell using 5.3 M LiFSA/TMP electrolyte. The initial coulombic efficiency was 95.8%, which is much higher than that of natural graphite. A 1C-rate corresponds to 372 mA g^{-1} on the weight basis of the graphite active material.

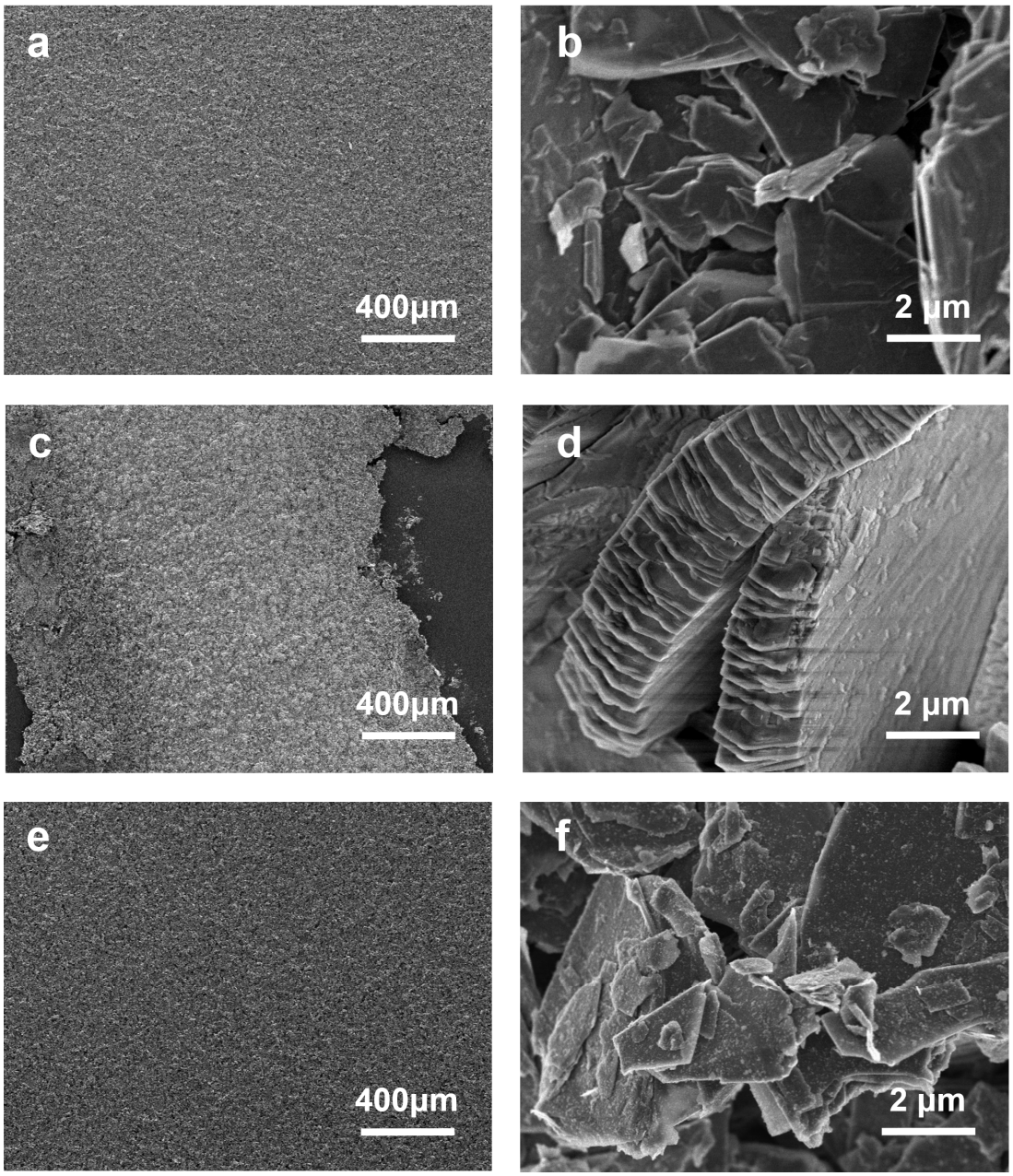

Supplementary Figure 16 | Surface morphology of the natural graphite electrodes. a,b, SEM images of the pristine graphite electrode before cycling. **c,d,** SEM images of the graphite electrode after one charge-discharge operation in the dilute 1.0 M LiFSA/TMP electrolyte. **e,f,** SEM images of the graphite electrode after several charge-discharge cycles in the concentrated 5.3 M LiFSA/TMP electrolyte. The dilute electrolyte caused the exfoliation of the graphite layered structure (**d**) and the electrode film (**c**), presumably due to the solvent cointercalation. By contrast, in the concentrated electrolyte, no significant change was observed on the surface morphology of the natural graphite electrode as compared to the pristine electrode, implying the formation of a uniform and robust passivation film on the surface.

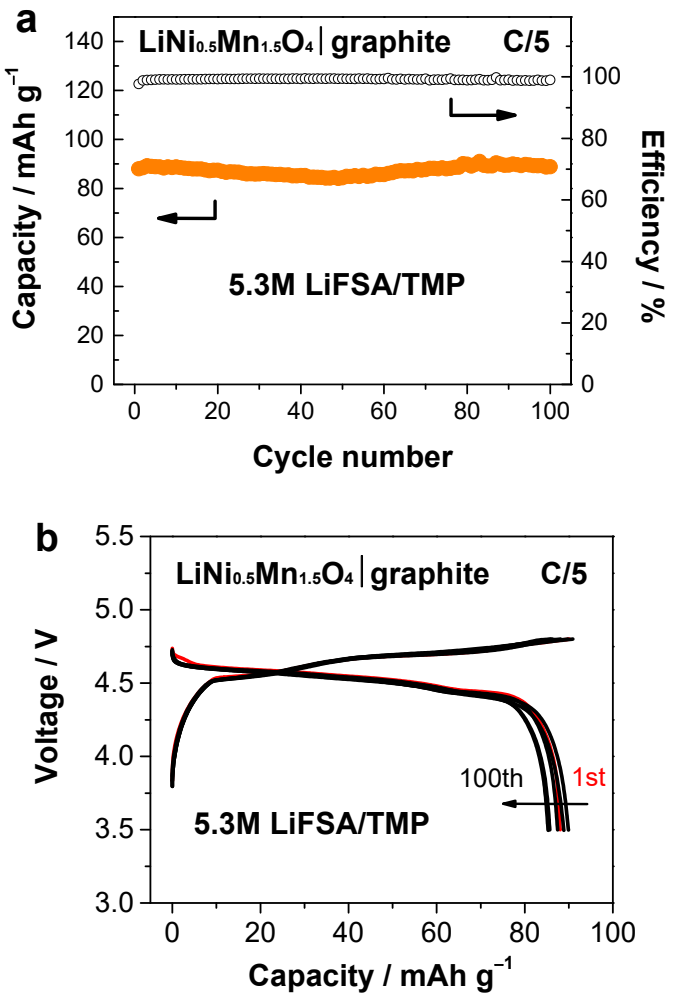

Supplementary Figure 17 | Electrochemical performance of a 5 V-class $LiNi_{0.5}Mn_{1.5}O_4$ | natural graphite full cell. a, Cycling performance and coulombic efficiency of the full cell using 5.3 M LiFSA/TMP electrolyte at a C/5 rate. **b**, Selected charge–discharge voltage curves for the full cell. Charge and discharge were conducted at the same C-rate at 25 °C after an initial ten cycles at an elevated temperature of 40 °C (to improve the wettability of the electrolyte toward the electrodes and separator). The cutoff voltage for all cycles was 3.5–4.8 V. A 1C-rate corresponds to 147 mA g^{-1} on the weight basis of the $LiNi_{0.5}Mn_{1.5}O_4$ active material. The capacity is based on the $LiNi_{0.5}Mn_{1.5}O_4$ cathode. There was little capacity decay together with a columbic efficiency of 99.2%, indicating that this nonflammable, fire-extinguishing electrolyte can be applied to the high-voltage lithium-ion battery. It should be noted that the capacity of the full cell can be considerably increased by using the artificial graphite instead of the natural graphite as the initial coulombic efficiency of the former is much higher than the latter.

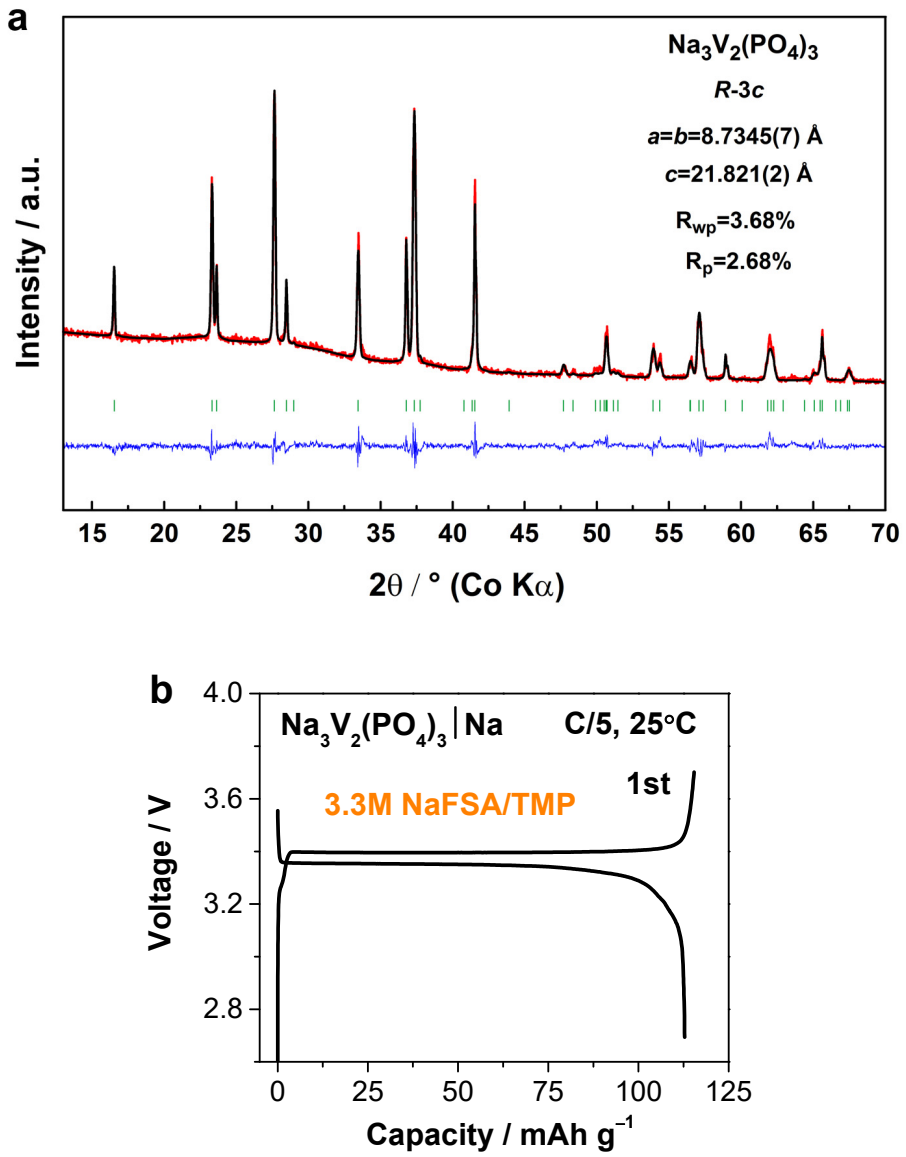

Supplementary Figure 18 | Structural characterizations and electrochemical property of the synthesized $Na_3V_2(PO_4)_3$. a, XRD pattern of as-synthesized $Na_3V_2(PO_4)_3$/C material. It indicates only one phase of $Na_3V_2(PO_4)_3$ without impurity. The residual conductive carbon is in an amorphous state. The detail crystallographic parameters of the as-synthesized $Na_3V_2(PO_4)_3$ (obtained from the Rietveld refinement) are listed in Supplementary Table 2. **b,** Initial charge-discharge profile of the $Na_3V_2(PO_4)_3$ | Na half-cell. These features in structure and electrochemical property are identical with the previous report.[11]

Supplementary Table 1 | XPS element analysis of surface products on the cycled hard carbon electrodes.

Element content (%)	S	N	P	O	F	Na
1.0 M NaFSA/TMP	0.4	0.1	15.8	54.7	1.8	27.2
3.3 M NaFSA/TMP	7.8	4.2	0.7	35.3	11.8	40.2

Note: The element analysis excludes carbon (C1s) because the hard carbon electrode itself also contributes to the C1s signal. The relative error is about 10%.

Supplementary Table 2 | Crystallographic parameters of the synthesized $Na_3V_2(PO_4)_3$.

Atom	Wyckoff site	*x*/*a*	*y*/*b*	*z*/*c*	Occupancy
Na(1)	6*b*	0	0	0	0.770
Na(2)	18*e*	0.633(2)	0	0.25	0.744
V	12*c*	0	0	0.1476(4)	1
P	18*e*	0.288(1)	0	0.25	1
O(1)	36*f*	0.183(2)	0.966(2)	0.1930(6)	1
O(2)	36*f*	0.190(2)	0.167(2)	0.0856(10)	1
Space group R -3 *c*	R_{wp} = 3.68%		R_p = 2.68%	R_{Bragg} = 6.31%	
a = *b* =8.7345(7) Å	*c* = 21.821(2) Å		*γ* = 120 °	*V* = 1441.7(3) Å^3	

Note: The errors of the calculated crystallographic parameters are shown in the brackets.

Supplementary References

1. McOwen, D. W. *et al.* Concentrated electrolytes: decrypting electrolyte properties and reassessing Al corrosion mechanisms. *Energy Environ. Sci.* **7,** 416–426 (2014).
2. Yamada, Y. *et al.* Unusual stability of acetonitrile-based superconcentrated electrolytes for fast-charging lithium-ion batteries. *J. Am. Chem. Soc.* **136,** 5039–5046 (2014).
3. Suo, L. *et al.* 'Water-in-salt' electrolyte enables high-voltage aqueous lithium-ion chemistries. *Science.* **350,** 938–943 (2015).
4. Wang, J. *et al.* Superconcentrated electrolytes for a high-voltage lithium-ion battery. *Nat. Commun.* **7,** 12032 (2016).
5. Wan, C. *et al.* Natural abundance ^{17}O, ^{6}Li NMR and molecular modeling studies of the solvation structures of lithium bis(fluorosulfonyl)imide/1,2-dimethoxyethane liquid electrolytes. *J. Power Sources* **307,** 231–243 (2016).
6. Fleutot, B., Pecquenard, B., Martinez, H., Letellier, M. & Levasseur, A. Investigation of the local structure of LiPON thin films to better understand the role of nitrogen on their performance. *Solid State Ionics* **186,** 29–36 (2011).
7. Joo, K.-H., Sohn, H.-J., Vinatier, P., Pecquenard, B. & Levasseur, A. Lithium Ion Conducting Lithium Sulfur Oxynitride Thin Film. *Electrochem. Solid-State Lett.* **7,** A256–A258 (2004).
8. http://www.organchem.csdb.cn
9. Komaba, S. *et al.* Electrochemical Na Insertion and Solid Electrolyte Interphase for Hard-Carbon Electrodes and Application to Na-Ion Batteries. *Adv. Funct. Mater.* **21,** 3859–3867 (2011).
10. Eshetu, G. G. *et al.* Comprehensive Insights into the Reactivity of Electrolytes Based on Sodium Ions. *ChemSusChem* **9,** 462–471 (2016).
11. Jian, Z. *et al.* Carbon coated $Na_3V_2(PO_4)_3$ as novel electrode material for sodium ion batteries. *Electrochem. commun.* **14,** 86–89 (2012).